

Sound of Interfacial Flows: Unraveling the Forces Shaping Fast Capillary Flows using their Acoustic Signature

Adrien Bussonnière^{1,2}, Arnaud Antkowiak¹, François Ollivier¹, Michaël Baudoin², and Régis Wunenburger¹

¹*Sorbonne Université, CNRS, Institut Jean le Rond d'Alembert, UMR 7190, F-75005 Paris, France*

²*Univ. Lille, CNRS, ECLille, ISEN, Univ. Valenciennes, UMR 8520 - IEMN, F-59000 Lille, France*

(Dated: February 2, 2022)

Many familiar events feature a distinctive sound: paper crumpling¹ or tearing², squeaking doors³, drumming rain^{4,5} or boiling water⁶. Such characteristic sounds actually carry a profusion of informations about the fleeting physical processes at the root of acoustic emission, which appears appealing especially in situations precluding direct or in-situ measurements, such as e.g. the rupture of micron-thick liquid sheet. Here we report on such a link between fast interfacial hydrodynamics and sound. The acoustic emission of a bursting soap bubble is captured by means of antennae and deciphered with the conceptual framework of aeroacoustics. This reveals that capillary forces, thin-film hydrodynamics, but also out-of-equilibrium surfactants dynamics all shape the capillary burst sound. Whereas ultra-fast imagery only captures the shapes of flows, the acoustic signature radiated by hydrodynamical forces offers a timely complement for it allows a direct experimental access to these dynamical quantities.

FORMS and forces in flows with interfaces are intertwined, notably because interfaces, more than just geometrical boundaries, exert forces. As Rayleigh noted in 1891, a trademark of these flows is that they “pass so quickly so as to elude ordinary means of observation”⁷. This represents of course a major hurdle in the experimental characterization of these interfacial flows, and this probably explains why their understanding has been so strongly linked to the development of imaging techniques, dating back to the rolling stroboscope of Savart which allowed to see the disintegration of a liquid stream into droplets⁸, the arising of spark photography at the end of the nineteenth century which revealed the instantaneous rupture of an underwater gas stream into bubbles⁷ or the shape of a splash⁹, the first ultra-fast camera that monitored the bursting of a soap bubble at 2,000 frames per second in 1907, tinkered with a rolling cardboard and repeated sparks in Etienne-Jules Marey workshop¹⁰ up to the development of modern ultra-fast imaging used since the fifties to capture splashes¹¹ and soap film rupture¹² and continuously developed since then (see Thoroddsen *et al.*¹³ for a review). If forms only provide a partial picture of these flows, it appears that a direct experimental access to the forces with e.g. the immersion of pressure sensors in thin rupturing films seems impracticable. Conversely, time-varying or moving forces radiate acoustic waves. Here we show on a model bursting soap bubble

experiment that these acoustic waves are detectable and that their analysis allows to find the locus of rupture of the bubble, and to give time-resolved informations about the thickness profile of the bubble, the inner thin-film hydrodynamics and dynamical change in surface tension due to surfactants reorganization across the bubble during bursting.

We set out by blowing air bubbles with a syringe pump using a 0.25 g/L sodium dodecyl sulfate (SDS)-water solution. The bubbles of 1 mL typical volume are placed atop a vertical capillary tube (see Fig. 1a). Bursting events are either spontaneous or triggered using a hydrophobic needle located 10 – 15 mm above the tube outlet, visible on top of the pictures of bursting bubble shown in Fig. 1 a. Air inside the bubble is known to be pressurized at Laplace overpressure $\Delta P_0 = 4\gamma_0/R$ by the two liquid-air interfaces constituting the soap film, $R \simeq 6$ mm being the bubble radius and $\gamma_0 = (50 \pm 1)$ mN · m⁻¹ the equilibrium surface tension of the soap solution at ambient temperature. Therefore, one would expect an acoustic emission with spherical symmetry resulting from the sudden overpressure release following the film bursting and a N-shaped pressure signal with duration $2R/c \simeq 35$ μ s ($c \simeq 340$ m · s⁻¹ is the speed of sound in air) similar to the popping sound of rubber balloons¹⁴ or to the blast wave of spherical explosions¹⁵. To test the validity of this picture, we image the bubble bursting using a high-speed camera and we record simultaneously its acoustic emission using arrays of microphones, which allow us to determine the associated radiation pattern. In a first series of experiments dedicated to the identification of the sources of sound we use three circular acoustic antennae each made of eight calibrated MEMS microphones (see Sup. Mat.) regularly distributed along a planar, circular frame coinciding with a meridian of the bubble and with radius 44 mm, 71 mm and 112 mm respectively, sketched in Fig. 1 b. The eight pressure signals recorded by the 44 mm radius antenna during the triggered bursting of a fresh bubble are shown in Fig. 1 c. Remarkably, although the signals exhibit the same shape, their sign and amplitude depend on MEMS colatitude θ (as defined in Fig. 1 b), the signals recorded above and below the bubble having opposite signs. Moreover, we note that acoustic emission lasts for 4 ms. The puzzling disagreement between our observations and the naive picture sketched previously of isotropic acoustic radiation by the bursting bubble can be resolved by focusing on the pictures of the bubble during the bursting event. As known since Bull¹⁶, bub-

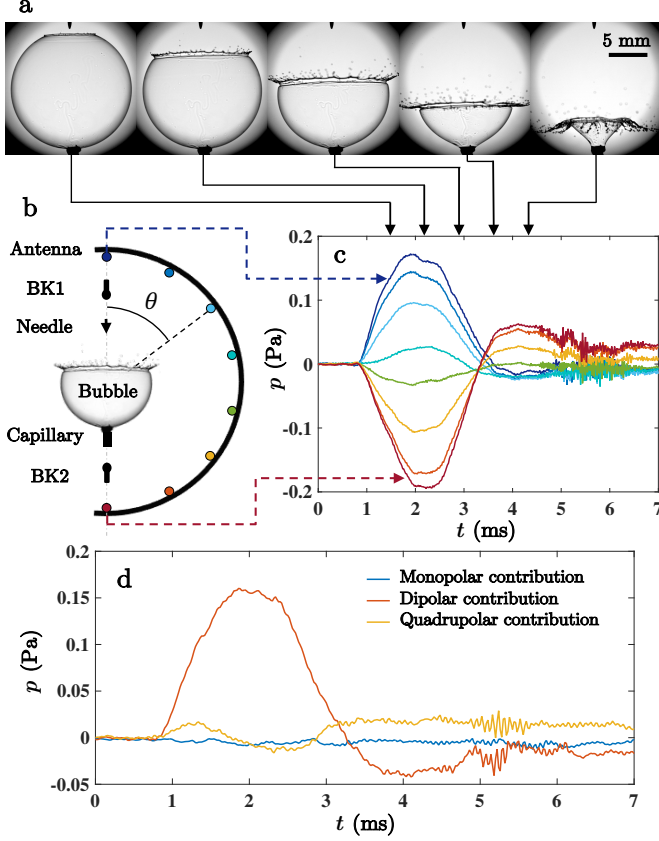


FIG. 1. **Directivity and dipolar nature of the acoustic emission.** **a**, High speed images of the bursting of a fresh 2 mL soap bubble triggered using a needle visible on top of the pictures. **b**, sketch of the setup showing one of the three circular acoustic antennae each made of eight MEMS microphones (coloured circles) used to measure the sound directivity and the two large bandwidth microphones labelled BK1 and BK2. **c**, the eight pressure signals acquired by the 44 mm radius acoustic antenna during bubble bursting. The acquisition times of the bubble pictures are indicated by black arrows. **d**, monopolar, dipolar and quadrupolar contributions to the pressure signal measured by the MEMS microphone located on the bubble top, computed from the 24 signals acquired using the acoustic antennae (see Sup. Mat.).

ble bursting usually begins with the spontaneous or triggered opening of a hole in the soap film followed by the growth of a circular rim gobbling up the soap film in its path at a typical speed $v_r \sim 10 \text{ m} \cdot \text{s}^{-1}$ up to its complete disappearance, as shown in the picture strip shown in Fig. 1 a. According to^{17–19}, as the film is pulled by surface tension and its acceleration is moderated by the inertia of the growing liquid rim, v_r is quantitatively predicted by¹⁹:

$$v_r = \sqrt{\frac{2\gamma_0}{\rho_f e_0}}, \quad (1)$$

where $\rho_f = 1.0 \times 10^3 \text{ kg} \cdot \text{m}^{-3}$ is the liquid film density and $e_0 \sim 1 \text{ } \mu\text{m}$ its typical thickness. The film retraction

is expected to last for $T = \pi R/v_r \simeq 5 \text{ ms}$, in agreement with observations. The comparison between the pictures of the bursting bubble and the synchronized recording of its acoustic signature, both displayed in Fig. 1 a and c, reveals that the bubble radiates sound during whole opening. This suggests that acoustic emission may be governed by liquid film retraction. Actually, the physical mechanism of sound radiation can be elucidated by referring to aeroacoustics theory, which classifies sound emission into three kinds of sources, monopolar sources associated to the injection of mass into the air, dipolar sources due to momentum injection, and quadrupolar sources mainly associated to air flow^{20–22}. Here, during the bubble opening, the sudden relaxation of the air compressed in the bubble is expected to result in a monopolar acoustic emission (i.e. with spherical symmetry) of duration T and pressure magnitude $p_M \sim \gamma_0 M^2/r$, where $M = v_r/c$ is the Mach number associated to the rim motion and r the distance between the bubble center and the detection point (see Sup. Mat.). Moreover, throughout the soap film retraction the stresses exerted by the soap film on the inner air $\Delta P_0 \mathbf{n}$ (\mathbf{n} is the unit vector normal to the film oriented toward the bubble center) do not balance, as illustrated in the enlargement *A* in Fig. 3 c. Their addition results in a capillary force $F\mathbf{e}_z$ directed upward (\mathbf{e}_z is the vertical unit vector oriented upward). As the distribution of capillary stresses is unsteady, so is the resulting capillary force accelerating the air and an acoustic emission pointing along the direction of momentum injection occurs in the form of a dipolar radiation of duration T with symmetry axis coinciding with the bubble center to initial hole axis, here the vertical. Given that here sound is recorded in the near-field of the acoustic source, i.e. at $r \lesssim cT$, the acoustic pressure amplitude associated to the dipolar radiation is $p_D \sim \gamma_0 R/r^2 \cos \theta$ (see Sup. Mat.). Finally, the air flow in the wake of the moving liquid rim should result in an acoustic emission of duration T with quadrupolar symmetry and acoustic pressure amplitude in the near-field $p_Q \sim \frac{R^2}{r^3} e_0 \rho_a v_r^2$, where $\rho_a = 1.2 \text{ kg} \cdot \text{m}^{-3}$ is air density (see Sup. Mat.). Given the investigated values of r and R , $p_M/p_D \sim \frac{r}{R} \frac{4}{3\pi^2} M^2 \sim 10^{-2}$ and $p_Q/p_D \sim \frac{R}{r} \frac{\rho_a}{\rho_e} \sim 10^{-4}$, which explains why the measured acoustic signature of a bursting bubble presented in Fig. 1 c appears as dipolar (conversely, this explains why bursting rubber balloons, which are actually torn along cracks commonly propagating at supersonic speeds even at moderate strains²³, have acoustic signatures that appear as monopolar¹⁴). This conclusion can be strengthened by computing the three pressure fields associated respectively to the monopolar, dipolar and quadrupolar radiations from the 24 signals acquired using the acoustic antennae using a signal processing detailed in Sup. Mat. The corresponding three multipolar contributions to the pressure signal measured by the MEMS microphone located on the bubble top are shown in Fig. 1 d. Their comparison confirms that the bubble acoustic emission is mainly dipolar, which leads us to focus on the dipolar radiation. According to Lighthill²¹, assuming the bubble

to disappear in the place, i.e. the film to remain spherical during bursting, away from the bubble, i.e. in the $r/R \gg 1$ limit, the acoustic pressure detected at distance r , colatitude θ and time laps t after the onset of bubble bursting can be approximated by:

$$p_D(r, \theta, t) = \frac{1}{4\pi r} \cos(\theta) \left[\frac{1}{c} \dot{F}(t') + \frac{1}{r} F(t') \right] \quad (2)$$

with:

$$F(t) = \pi R^2 \Delta P_0 \sin^2[\theta_r(t)] \quad (3)$$

$\theta_r(t)$ being the time-dependent colatitude of the retracting liquid rim, as defined in Fig. 2 a, $t' = t - r/c$ the retarded time and \dot{F} the derivative of F (see Sup. Mat.). In the frame of this simple model of bubble disappearance in the place by rim retraction, the capillary force varies only because the retracting rim continuously reduces the film surface area. Correlatively, the source of sound coincides with the rim.

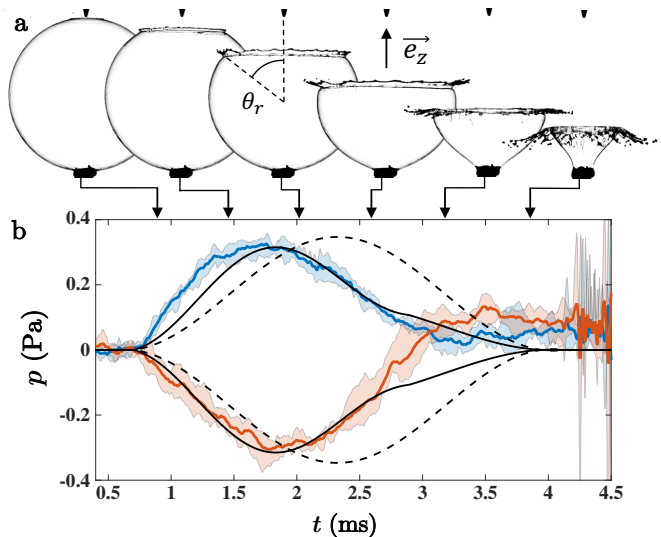


FIG. 2. **Confrontation with models of acoustic emission in the case of fresh bubbles.** **a**, high-speed images of the bursting of a 1 mL, fresh bubble triggered by a needle. **b**, pressure signals acquired during the bursting of a 1 mL, fresh soap bubble by top BK1 (blue curve) and bottom BK2 (red curve) microphones distant of 30 mm from the bubble center, averaged over five bursting events, the shaded areas being bounded by the maximum and minimum of the five signals. Dashed black curve: model accounting for acoustic emission by the retracting rim only (Eqs. 2, 3). Solid black curve: model accounting for additional acoustic emission by the thickness shock wave propagating along the soap film (Eqs. 2, 6).

To quantitative test the validity of this model, in a second series of experiment we use two large bandwidth microphones (see Sup. Mat.) distant of $r = 30$ mm from a $R = 6.2$ mm bubble, i.e. in its near-field, and positioned above and below the bubble, named BK1 and

BK2 in Fig. 1. The two acoustic pressure signals acquired during the triggered burst of a fresh bubble are compared to their prediction using Eqs. 2 and 3 in Fig. 2 b. $\theta_r(t)$ has been first extracted from the images of bubble bursting shown in Fig. 2 a and then interpolated at acoustic sampling frequency. The model catches the shape and amplitude of the measured signals but overestimates their duration and maximal amplitude by approximately 30 % and 10 % respectively. As shown in the following, the limitation of this model does not rely on the description of the acoustic emission process but actually on the roughness of the description of the film dynamics adopted up to now.

To describe the film dynamics more accurately, a time-resolved mapping of its thickness distribution during bursting is required. To this aim, long-lived bubbles are considered. Interestingly, due to gravity-driven drainage, long-lived bubbles indeed exhibit strong vertical thickness stratification and film thinning down to thicknesses comparable to optical wavelengths. Consequently, when illuminated by a source of white light and observed in transmission, long-lived bubbles display light interference fringes (see Fig. 3 a) from which the film thickness distribution can be determined just before and during bursting (see Sup. Mat.).

After typically one minute of lifetime, long-lived bubbles ultimately spontaneously burst by opening at their top where the film is the thinnest (see Fig. 3 a). Consequently, the two microphones are always located along their axis of symmetry, as in needle-triggered bursting experiments. The detected acoustic signals, shown in Fig. 3 d, are initially much steeper than in the case of fresh bubbles. This may be ascribed to the initially large retraction velocity $v_r \propto e_0^{-1/2}$ (see equation 1) of the thin film located on the bubble top combined with the dependence of the radiated sound on $\dot{F} \propto \dot{\theta}_r = v_r/R$ (see equation 2). Once the actual rim colatitude evolution $\theta_r(t)$ determined by image analysis and interpolated, the model based on Eqs. 2, 3 can be used to predict these acoustic signals. As shown in Fig. 3 d, the agreement between experimental data and their prediction is qualitative, although satisfactory, as in the case of fresh bubbles.

A careful observation of the light interference pattern displayed by long-lived bursting bubbles during bursting reveals that, starting from the hole, a thickness discontinuity propagates along the film downward ahead of the rim, as indicated by red arrow tips in the pictures shown in Fig. 3 a. The generation of such a thickness shock wave during the retraction of soap films is commonly observed, in particular along planar films made of the same soap solution¹⁹. The decrease of the soap film area resulting from the rim retraction indeed induces a rapid compression of the surfactants located at the film surface. Since their desorption kinetics is generally slow compared to the film retraction velocity, surfactants behave as if they were insoluble²⁴. Consequently they are carried along the compressed films and concentrate. Due to this rapid

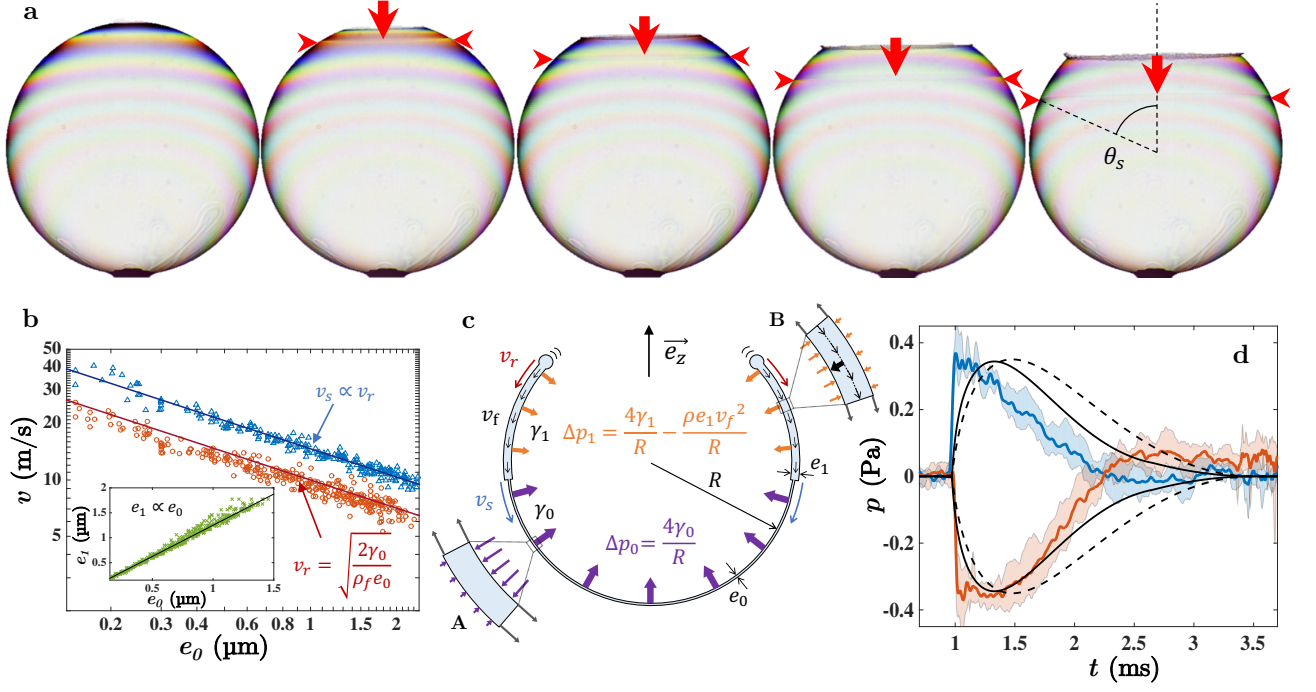


FIG. 3. Observation of the thickness shock wave propagating along bursting long-lived bubbles and implications on the acoustic signature. **a**, High-speed images of the spontaneous bursting of a long-lived, 0.5 mL soap bubble illuminated by a source of white light evidencing the propagation of a thickness shock wave downward ahead of the retracting rim, as indicated by red arrow tips. **b**, Variations of the thickness shock wave velocity v_s (blue symbols) and of the rim velocity v_r (red symbols) as function of the equilibrium film thickness e_0 , evidencing that $v_s \propto v_r$ and demonstrating the validity of equation (1). Inset: variation of soap film thickness between the shock wave and the rim $e_1(\theta, t)$ as function of the equilibrium film thickness $e_0(\theta)$, evidencing that e_1 is independent of time and $e_1 \propto e_0$. **c**, Sketch of the bursting soap bubble showing the rim retracting at velocity v_r (red arrow), the thickness shock wave propagating at velocity v_s (blue arrow) downward ahead of the rim and the thickened film flowing at velocity v_f (black arrows) behind the shock wave. The capillary stresses with amplitude Δp_0 (respectively Δp_1) exerted on the air by the film at rest (resp. by the flowing film) with thickness e_0 (resp. e_1) are represented as violet (resp. orange) arrows. Enlargement A: portion of the film at rest and at equilibrium showing the different pressure stresses (violet arrows) exerted by inner and outer air. Enlargement B: portion of the out-of-equilibrium, moving film showing the flow velocity (black arrows), the centripetal acceleration (bold, black arrow), the unchanged outer pressure stresses and the reduced inner pressure stresses (orange arrows). **d**, pressure signals acquired during the bursting of 0.5 mL, long-lived soap bubbles by top BK1 (blue curve) and bottom BK2 (red curve) microphones distant of 30 mm from the bubble center, averaged over three bursting events, the shaded areas being bounded by the maximum and minimum of the three signals. Dashed black curve: model accounting for acoustic emission by the retracting rim only (Eqs. 2, 3). Solid black curve: model accounting for additional acoustic emission by the thickness shock wave propagating along the soap film. (Eqs. 2, 6).

surfactant concentration, the surface tension of the compressed films decreases and departs from its equilibrium value. Depending on the out-of-equilibrium surface tension versus surface compression relation specific to the surfactant, a thickness and surface tension shock wave may appear²⁵, as sketched in Fig. 3 c, which is the case for SDS in our experiments and in¹⁹.

The occurrence of a thickness shock wave during bubble bursting experiments is expected to affect acoustic emission in several aspects. First, recalling that acoustic emission originates from the unsteadiness of the capillary stresses, we identify this surface tension discontinuity propagating in front of the rim as a supplementary source of sound. More specifically, the surface tension drop behind the thickness shock wave tends to increase the capillary force exerted by the bubble on the inner air

(and hence the acoustic emission) when the shock wave is located in the upper hemisphere ($\theta < \pi/2$), as sketched in Fig. 3 c, and to decrease it in the lower hemisphere ($\theta > \pi/2$), in agreement with the observed evolution of the sign of the difference between the experimental signals and their prediction based on Eqs. 2, 3 shown in Fig. 3 d.

Moreover, the shock wave triggers a flow of the soap film that further decreases the capillary stresses, as demonstrated in the following. Assuming a thickness shock wave located at colatitude $\theta_s(t)$ to propagate at velocity v_s along a film initially at rest and at equilibrium, surfactant effective insolubility assumption, mass conservation and momentum balance across the shock indeed entail the motion of the whole film behind the shock wave at velocity $v_f(\theta_s^-)$ that satisfies the following

relations²⁵:

$$v_f(\theta_s^-) = v_s \left[1 - \frac{e_0(\theta_s^+)}{e_1(\theta_s^-)} \right], \quad (4)$$

$$2 [\gamma_0(\theta_s^+) - \gamma_1(\theta_s^-)] = \rho_f e_0(\theta_s^+) v_f(\theta_s^-) v_s, \quad (5)$$

where $e_0(\theta_s^+)$ is the thickness of the film at rest and at equilibrium in front of the shock wave, $e_1(\theta_s^-)$ and $\gamma_1(\theta_s^-)$ the thickness of the compressed film and its out-of-equilibrium surface tension behind the shock wave, respectively. Consequently, behind the shock, each moving fluid element runs a circular trajectory with radius R around the bubble center at tangential velocity v_f and is thus subjected to the centripetal acceleration v_f^2/R . Application of second Newton's law to such an accelerated fluid element with thickness e_1 submitted to external pressure P_0 , internal pressure P_{in} and surface tension γ_1 , as sketched in the enlargement B in Fig. 3 c, reveals that the centripetal acceleration of the moving film noticeably reduces the overpressure it exerts on the inner air, i.e. $P_{in} - P_0 = \Delta P_1 = 4 \gamma_1/R - \rho_f e_1 v_f^2/R < 4 \gamma_1/R$. Such an influence of the in-plane film motion on the pressure jump across curved films is known to be responsible of the large variety of shapes of water bells^{26–29}.

All the quantities involved in this description of the soap film dynamics can be experimentally assessed by analysing the light interference patterns displayed by the bubble. First, the rim colatitude $\theta_r(t)$, the shock wave colatitude $\theta_s(t)$, the film thickness distribution $e_0(\theta)$ along the film at equilibrium and at rest and the film thickness distribution $e_1(\theta, t)$ along the out-of-equilibrium, flowing film behind the shock are experimentally determined from image analysis. Next, neglecting the weak departure to sphericity of the film during its retraction, the rim and shock wave velocities are calculated using $v_r = R\dot{\theta}_r$ and $v_s = R\dot{\theta}_s$. Finally, $v_f(\theta_s^-)$ and $\gamma_1(\theta_s^-)$ are calculated using Eqs. 4, 5. The agreement between the experimental variation of $v_r(\theta_r)$ with $e_0(\theta_r)$ and its prediction using equation (1), both shown in Fig. 3 b, demonstrates the validity of equation (1) along a curved and stratified soap film. As also shown in Fig. 3 b, $v_s \simeq \alpha v_r$ with $\alpha = 1.57$, in quantitative agreement with previous measurements performed along planar soap films¹⁹. Next, the dependence of $e_1(\theta, t)$ versus $e_0(\theta)$ all along the moving film, plotted in the inset of Fig. 3, is found to be linear and exhibits little scattering, indicating that e_1 does not basically depend on time and satisfies $e_1(\theta) \simeq \beta e_0(\theta)$ with $\beta = 1.27$. As detailed in Supp. Mat., from these experimental results it can be shown that, given the validity of equation (1) and since v_s/v_r and e_1/e_0 are constant along the moving film, $v_f(\theta_s^-)$ and $\gamma_1(\theta_s^-)$ can be determined from the sole measurement of the rim retraction kinetics $\theta_r(t)$ and the independent measurement of γ_0 using Eqs. 4, 5. Finally, as detailed in Supp. Mat., surfactant insolubility assumption allows one to show that ΔP_1 is constant all along the moving film. This leads us to conclude that the only sources of unsteadiness of the capillary stresses, and therefore of acoustic emission, are the moving rim and shock wave. The capillary stresses

along the bursting bubble being constant equal to ΔP_1 in the range $\theta \in [\theta_r(t); \theta_s(t)]$ and to ΔP_0 in the range $\theta \in [\theta_s(t); \pi]$, their addition results in the following capillary force exerted by the soap film on the inner air:

$$F(t) = \pi R^2 \{ (\Delta P_0 - \Delta P_1) \sin^2 [\theta_s(t)] + \Delta P_1 \sin^2 [\theta_r(t)] \} \quad (6)$$

from which the acoustic emission away from the bubble can be evaluated using equation (2). The agreement between the acoustic signals detected by BK1 and BK2 microphones during the bursting of long-lived bubble and their prediction using equation (6), shown in Fig. 3 d, is more satisfactory than using equation (3), in particular regarding the signal duration.

Extrapolating this refined description of film dynamics to fresh bubbles allows one to predict and to quantitatively describe the propagation of a thickness shock wave along bursting fresh bubbles, although they are made of thick films that display no light interference fringes and hardly visible shock waves. This is possible because the whole description of the film dynamics requires only the knowledge of the rim colatitude $\theta_r(t)$ that is as easily measurable on fresh bubbles as on long-lived ones. When applying this refined model of acoustic emission (Eqs. 2, 6) to fresh bubbles, one observes a quantitative agreement between the acoustic signals measured during the needle-triggered bursting of fresh bubbles and their prediction, as shown in Fig. 2 b. This confirms that the thickness shock wave propagating along the bursting soap film noticeably contributes to sound emission in the case of fresh bubbles too. Thanks to this thorough study, we have shown that the description of the acoustic emission by a bursting bubble we propose is fully consistent with the current understanding of soap film retraction dynamics.

This study has revealed the profusion of information on bubble bursting carried by the sound radiated during the event and accessible using aeroacoustics theory. In particular, we could reveal the acoustic signature of the thickness shock wave propagating along the bursting soap film. As exemplified by this study of a specific hydrodynamic event, dipolar acoustic radiation can inform us about the forces at play during the rapid evolution of liquid interfaces and more generally during violent events, thus potentially constituting a precious diagnostic complementary to high-speed imaging that primarily reveals shapes. However, such an acoustic radiation constitutes only a tiny record of the violence of the bubble bursting event and not a mechanism of energy loss, since the ratio of the total acoustic energy radiated to the variation of surface energy^{30,31} is smaller than 10^{-6} , see Supp. Mat. for details.

Methods

Soap bubble production. Sodium dodecyl sulfate (SDS) from *Euromedex* was used as surfactant and was diluted in distilled water down to 0.25 g/L. The surface tension of the solution was measured using the du Noüy ring method. 1.5 μ L droplets of the soap solution were carefully deposited on top of a vertical capillary tube using a micropipette. To limit the draining of the solution before bubble inflation, the end of the tube was thickened using a rim of glue.

Bubbles were then inflated at a calibrated volume using a syringe pump with a rate of 20 mL/min. For triggering the bursting of fresh bubbles, a hydrophobic Rain X[®]-coated needle was positioned vertically at a distance of $2R$ above the capillary end.

Video and sound recordings. High-speed imaging of bursting bubbles was performed using a *Photron Fastcam SA5* camera

at a 20 000 fps rate when color movies were required and a *Vision Research Phantom V711* camera at a 25 000 fps rate for the black and white movies. Video and sound recordings were synchronized by triggering the acquisition of the acoustic signals once the bubble top disappeared on the bubble pictures using the Image Triggering function of the camera software.

-
- ¹ P. A. Houle and J. P. Sethna, Phys. Rev. E **54**, 278 (1996).
 - ² L. I. Salminen, A. I. Tolvanen, and M. J. Alava, Phys. Rev. Lett. **89**, 185503 (2002).
 - ³ S. M. Rubinstein, G. Cohen, and J. Fineberg, Nature **430**, 1005 (2004).
 - ⁴ G. J. Franz, J. Acoust. Soc. Am. **31**, 1080 (1959).
 - ⁵ L. Gordillo, T.-P. Sun, and X. Cheng, J. Fluid Mech. **840**, 190 (2018).
 - ⁶ S. Aljishi and J. Tatarkiewicz, Am. J. Phys. **59**, 628 (1991).
 - ⁷ L. Rayleigh, Nature **44**, 249 (1891).
 - ⁸ F. Savart, Ann. Chim. Phys. **53**, 337 (1833).
 - ⁹ A. Worthington, *A study of splashes* (Longmans, Green and co., 1908).
 - ¹⁰ T. Lefebvre and L. Mannoni, 1895 Mille huit cent quatre-vingt-quinze **18**, 144 (1995).
 - ¹¹ O. G. Engel, J. Res. Nat. Bur. Stand. **54**, 281 (1955).
 - ¹² W. E. Ranz, J. Appl. Phys. **30**, 1950 (1959).
 - ¹³ S. Thoroddsen, T. Etoh, and K. Takehara, Ann. Rev. Fluid Mech. **40**, 257 (2008).
 - ¹⁴ D. T. Deihl and J. F. Roy Carlson, Am. J. Phys. **36**, 441 (1968).
 - ¹⁵ G. B. Whitham, *Linear and nonlinear waves*, Vol. 42 (John Wiley & Sons, 1999).
 - ¹⁶ L. Bull, Institut E.-J. Marey (1904).
 - ¹⁷ G. I. Taylor, Proc. R. Soc. Lond. A **253**, 313 (1959).
 - ¹⁸ F. E. C. Culick, J. Appl. Phys. **31**, 1128 (1960).
 - ¹⁹ W. R. McEntee and K. J. Mysels, J. Phys. Chem. **73**, 3018 (1969).
 - ²⁰ P. M. Morse and K. U. Ingard, *Theoretical acoustics* (Princeton university press, 1968).
 - ²¹ J. Lighthill, *Waves in Fluids* (Cambridge University Press, 2001).
 - ²² M. Howe, *Acoustics and Aerodynamic Sound* (Cambridge University Press, 2014).
 - ²³ S. Moulinet and M. Adda-Bedia, Phys. Rev. Lett. **115**, 184301 (2015).
 - ²⁴ B. R. Vijayendran, J. Phys. Chem. **79**, 2501 (1975).
 - ²⁵ S. Frankel and K. J. Mysels, J. Phys. Chem. **73**, 3028 (1969).
 - ²⁶ F. Savart, Ann. Chim **54**, 56 (1833).
 - ²⁷ F. Savart, Ann. Chim. **54**, 113 (1833).
 - ²⁸ J. Boussinesq, CR Acad. Sci. Paris **69**, 45 (1869).
 - ²⁹ G. I. Taylor, Proc. R. Soc. Lond. A **253**, 289 (1959).
 - ³⁰ A. B. Pandit and J. F. Davidson, J. Fluid Mech. **212**, 11 (1990).
 - ³¹ P.-G. de Gennes, Faraday Discuss. **104**, 1 (1996).